Dyes and Pigments 92 (2011) 705–713

Contents lists available at ScienceDirect

Dyes and Pigments

journal homepage: www.elsevier.com/locate/dyepig

Spectrophotometric investigations and computational calculations of prototropic tautomerism and acid–base properties of some new azo dyes

Y.H. Ebead*

South Valley University, Faculty of Science, Chemistry Department, 83523 Qena, Egypt

ARTICLE INFO

Article history:
Received 12 December 2010
Received in revised form
25 May 2011
Accepted 2 June 2011
Available online 15 June 2011

Keywords:
Azo dyes
Prototropic tautomerism
DFT calculations
Acid–base properties
UV–Vis spectra
HOMO

ABSTRACT

The prototropic tautomerism in four novel azo compounds derived from pyrazolo[1,5-*a*]*pyrimidin*-7(4H)-one was intensively examined. Tautomeric structures which result from annular and azo-hydrazone tautomerism were exposed to semiempirical and density functional theory (DFT) calculations, allowing the recording of structural parameters, physicochemical properties and equilibrium constants to be recorded. The values of the equilibrium constants determined among the most stable forms clearly showed that compounds **1** and **2** co-exist in the NH and hydrazone forms. However, NH tautomers were strongly preferred to other forms in compounds **3** and **4**. The observed electronic absorption bands were assigned and compared with the predicted transitions using a time-dependent DFT method (TDDFT). In all solvents employed, except for DMF and acetonitrile, compounds **1** and **2** exhibited azo-hydrazone tautomerism. However, the ionized species were predominant in highly polar solvents for compounds **3** and **4**. In DMF, all the investigated dyes exist either in acid–base equilibrium or in the ionized form depending on the molecular structure. Hence, the values of the ionization constant (K_{ion}) and Gibbs free energy (ΔG) of the equilibrium existing in solution were calculated. In addition, the pK_a values of the investigated dyes were determined spectrophotometrically.

1. Introduction

Recently, many publications concerning the azo dyes – which are aromatic compounds bearing one or more –N=N– groups – in several topics have appeared in the literature. This is due to their biochemical and physicochemical properties as well as their wide applications in many other fields [1–10]. Thanks to their reactivity to form covalent bonds with OH, NH and SH groups in fibers, this group of compounds presents 70% by weight of the total amount of the dyes produced annually [11]. Notably, azo-hydrazone, annular tautomerism and other tautomeric structures that exist in the azo compounds have been extensively attempted by several researchers to recognize their exact geometrical structures and stability in gaseous phase (theoretically) and in the presence of solvent molecules [12,13]. This information is crucial for understanding their biological activity [14,15] and many other characteristics related to the structure such as their optical stability [16,17] and complex formation [18,19]. In this respect, spectrophotometric measurements and theoretical calculations turned out to be extremely useful for determining the molecular geometry especially when the X-ray data is not available [20,21]. In addition to the usefulness of the azo dyes themselves, their complexes with various metal ions are well documented as photochemical molecular devices, light sensitive probes in biological systems and photosensitizers in redox reactions [22]. Furthermore, biological and medicinal activities of pyrazolo[1,5-*a*]pyrimidines have stimulated considerable interest in the synthesis of derivatives of this ring system [23–25].

The knowledge of pK_a values provides a basis for understanding the chemical reactions between the compound of interest and its pharmacological target [26,27]. Additionally, they play a major role in acid–base titrations, complex formation and various analytical procedures. Also, the pK_a value(s) of a compound influences many characteristics such as its reactivity, spectral properties (color) and determination of the activity centers of enzymes in biochemistry [28]. Consequently, several publications were devoted for the determination of pK_a experimentally and theoretically [29–32]. The current piece of work covering the electronic absorption spectra, computational calculations and acid–base properties of four selected azo compounds (Scheme 1) as well as focusing on the influence of the substituent at C_5 of compounds **1**–**4** on the stability of different tautomers in solvents of variant polarities. A second aim is to work out the main structural and physicochemical features of these compounds and to indicate their applications. Last, the study drives at finding how far experimental findings are reflected in the

* Tel.: +20108928365; fax: +20965213383.
E-mail address: ebeadhassan88@yahoo.com.

0143-7208/$ – see front matter © 2011 Elsevier Ltd. All rights reserved.
doi:10.1016/j.dyepig.2011.06.005

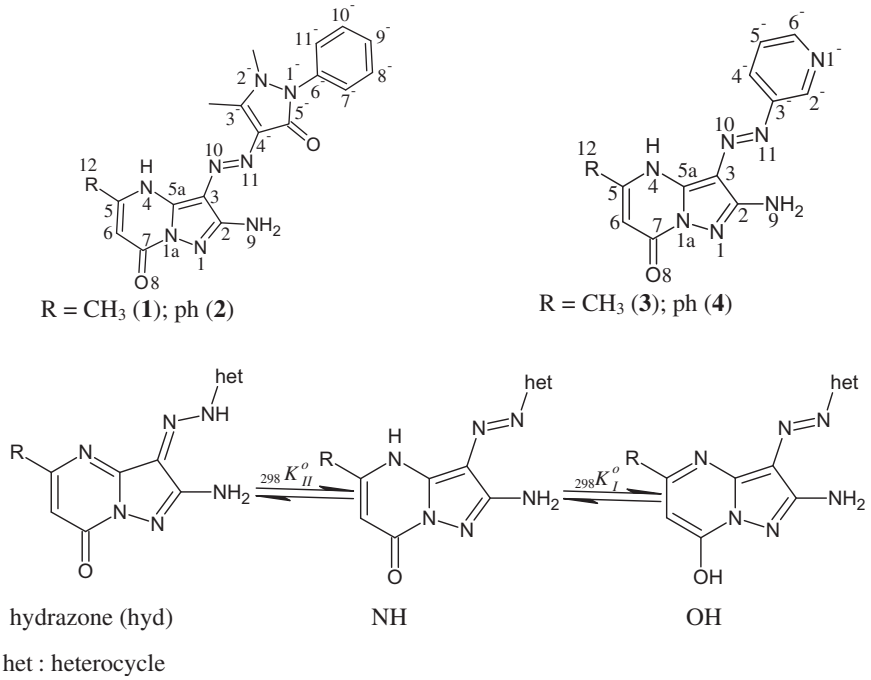

Scheme 1. Compounds and equilibria ($_{298}K^{o}$, equilibrium constant) investigated with the number of atoms indicated.

theoretical predictions and what information can be extracted from spectroscopic investigation. However, the usefulness of electronic spectroscopy in studying the tautomeric phenomena of this group of compounds and other potential biologically compounds has been demonstrated earlier [33–35].

2. Experimental

2.1. Compounds

2-amino-5-methyl-3-(2′,3′-dimethy-5′-oxo-1`-phenyl-3′-pyrazolin-4′-yl-diazinyl)pyrazolo[1,5-*a*]*pyrimidine*-7-(4*H*)-one (**1**), 2-amino-5-phenyl-3-(2′,3′-dimethy-5′-oxo-1′-phenyl-3′-pyrazolin-4′-yl-diazinyl)pyrazolo[1,5-*a*]*pyrimidine*-7-(4*H*)-one (**2**), 2-amino-5-methyl-3-(3′-pyridyldiazinyl)pyrazolo[1,5-*a*]*pyrimidine*-7-(4*H*)-one (**3**) and 2-amino-5-phenyl-3-(3′-pyridyldiazinyl)pyrazolo[1,5-*a*]*pyrimidine*-7-(4*H*)-one (**4**) (Scheme 1) were synthesized as previously reported [36].

2.2. Solutions and measurements

Stock solutions (1×10^{-3} mol dm^{-3}) of the compounds were prepared by dissolving a known weight of the solid in the required volume of each solvent; more dilute solutions were then obtained by accurate dilution with the proper solvent. pH control was achieved by using modified universal buffer solutions [37]. To account for differences in acidity, dielectric constant and ion activities in partially aqueous media relative to pure aqueous solutions, where the pH meter is standardized using aqueous buffers at 25 °C. The pH values in the former media were corrected by using the procedure described by Douheret (eq. (1)), where the meter reading $pH_{(R)}$ obtained in each water + organic solvent mixture differs by amount δ from the corrected reading pH^* [38].

$$pH^* = pH_{(R)} - \delta \quad (1)$$

The electronic absorption spectra were recorded on a Shimadzu 2401 PC spectrophotometer using 1-cm matched quartz cells within the wavelength range of 200–700 nm. The pH measurements were carried out using a Jenway 3051 pH meter accurate to ±0.01 pH unit. All measurements were carried out at 25 °C and temperature control was achieved using an ultrathermostat of accuracy ±0.05 °C.

2.3. Quantum chemical calculations

The full geometrical optimization of the isolated molecules **1**–**4** (Scheme 1) in the gas phase were carried out at the level of semi-empirical PM6 method [39], as well as density functional theory (DFT) [40] using a gradient technique [41,42] and 6-31G** [43,44] basis set. The DFT calculations were carried out with the B3LYP functional, in which Becke's nonlocal exchange [45,46] and the Lee–Yang–Parr correlation functionals [47] were applied. After the completion of the optimization, the Hessian (second derivatives of the energy as a function of the nuclear coordinates) was calculated and checked for positive definiteness to assess whether the structures were true minima [40,48]. The harmonic vibrational frequencies were then derived from the numerical values of these second derivatives and used to obtain the Gibbs' free energy contributions at 298.15 K and standard pressure. Structural parameters (bond lengths and dihedral angels) were extracted directly from the data files following the geometry optimizations. The solvent effect was included in the single-point DFT calculations utilizing the polarized continuum model (PCM) [49,50]. Natural atomic charges were obtained from NBO analysis [51]. The calculated visible absorption maxim (λ_{max}) of various tautomers have been also obtained by employing the TDDFT/6-31 G** calculations. Calculations at the PM6 level were carried out using MOPAC 2009 – free license on internet [52]. *Ab initio* calculations were performed using GAUSSIAN 03 for Windows program package [53]. All calculations were done on a Pentium IV PC computer.

3. Results and discussion

3.1. Structure and physicochemical properties

The transfer of the hydrogen atom connected to N_4 either to the keto-oxygen (O_8) or to N_{11} creates annular and azo-hydrazone

tautomerism, respectively (Scheme 1). In addition, it is well-known that a variety of azo dyes can co-exist in acid–base equilibrium particularly in basic solvents [54–56]. The ionization process is responsible for the change of the electron density of the whole molecule; therefore the ionized forms of the azo dyes examined have been further taken into account. Computations were performed for all possible structures of compounds **1**–**4** involved in Scheme 1 in the gaseous phase and in different solvents. Table 1 compiles selected structural parameters obtained only by geometrical optimization – since no experimental geometrical data are available in the literature – for NH, OH and hydrazone tautomers calculated at DFT and PM6 levels.

Obviously, the magnitude of the N_{10}=N_{11} bond length in the NH and OH forms is longer than the typical value (1.24 Å [57]), suggesting a considerable electron delocalization on the azo linkage. However, in the hydrazone tautomers the N_{10}–N_{11} bond is somewhat shorter than the standard single bond length (1.40 Å), which suggests a partially double bond character of it. This peculiarity can be explained as this bond is in fact a hybrid of the NH and hydrazone tautomers. The double-single bond character of the N_{10}–N_{11} bond confirms the proposed NH-hydrazone tautomerism process observed in the subsequently discussed electronic absorption spectral investigation. Both the computational levels indicate that the length of N_4–C_5 bond in the NH and hydrazone tautomers is significantly shorter than the ideal single bond (1.44 Å [57]), though it is longer than the standard double bond in the OH form (1.28 Å). This is presumably due to the participation of the nitrogen pair of electrons in the pyrazolopyrimidine ring resonance structure. This finding is in line with the recent X-ray results of some pyrazolopyrimidines [58] and adds a further evidence of electron delocalization over almost the whole molecule. Likewise, the results of the calculated C_6–C_7 and C_7–O_8 bond lengths clearly show that they fall between formally single and double bond character. This means that these bonds are implied in the ring resonance structure [59]. As can be seen from Table 1, the magnitude of the corresponding bond lengths in compounds **1**–**4** is slightly affected by the substituent at C_5. Interestingly, PM6 calculations are rather close to the standard bond length values to some extent compared to the calculated geometrical parameters extracted from DFT. Even though the later method reproduces values compared favorably to X-ray measurements of related azo compounds [60–63].

Analysis of the spatial structure of the dyes **1**–**4** has revealed that the fused heterocyclic fragment is completely planar in both NH and OH forms but deviates slightly from planarity in the hydrazone tautomers as the torsion $C_6C_7N_{1a}N_1$ angle shows (Table 1). The torsion angle between the plane of the pyrazolo[1,5-*a*]*pyrimidine*-7-(4*H*)-one and azo linkage ($C_2C_3N_{10}N_{11}$) is essentially planar in both OH and hydrazone forms. In molecules **1** and **2**, the dihedral angle $N_{10}N_{11}C_4^-C_5^-$ shows that the antipyrine fragment and the azo linkage in the hydrazone forms lie nearly almost in one plane. Similarly, the values of such angle ($N_{10}N_{11}C_3^-C_2^-$) in compounds **3** and **4** indicate that the pyridine moiety lies in one plane with the main skeleton in the OH tautomers. However, the central unifying structural feature in all tautomeric forms is the deflection of the phenyl substituent at C_5 and N_1^- from the main plane in compounds **1**, **2** and **4** (this is reflected by the values of the torsion angles $C_6C_5C_{12}C_{13}$ in the case of compounds **2**, **4** and $N_2^-N_1^-C_6^-C_7^-$ in compound **1**). On the other side, these forms are completely planar with respect to the remaining compound (**3**). This confirms the considerable conjugation taking place throughout the whole molecule.

As can be seen from Table 2, the NH tautomers exhibit the lowest energy value among all the potential tautomers calculated at the B3LYP/6-31G** computational level. In the same stream, the OH

Table 1
The calculated (DFT, PM6) structural parameters (bond length in Å, angles in degree) of compounds **1**–**4**.

Compound	Parameter	DFT			PM6		
		NH	OH	hyd	NH	OH	hyd
1	N_4C_5	1.380	1.330	1.379	1.403	1.352	1.406
	C_6C_7	1.462	1.385	1.452	1.457	1.393	1.451
	C_7O_8	1.215	1.340	1.219	1.201	1.356	1.204
	$N_{10}N_{11}$	1.281	1.281	1.314	1.265	1.265	1.309
	$N_{10}N_{11}C_4^-C_5^-$	−174.887	−177.839	−179.185	−173.697	−178.991	−179.366
	$C_6C_7N_{1a}N_1$	−179.661	−179.861	178.404	−179.879	−179.942	−178.588
	$C_2C_3N_{10}N_{11}$	1.074	−0.297	−0.732	4.359	1.692	−2.112
	$N_2^-N_1^-C_6^-C_7^-$	−162.192	161.417	21.021	−166.871	−167.524	−165.775
2	N_3C_4	1.381	1.336	1.380	1.401	1.349	1.406
	C_5C_6	1.460	1.385	1.450	1.458	1.392	1.454
	C_7O_8	1.216	1.340	1.219	1.201	1.356	1.204
	N_9N_{10}	1.281	1.281	1.313	1.265	1.265	1.308
	$N_{10}N_{11}C_4^-C_5^-$	−176.320	−178.947	−179.148	−174.948	−177.697	−179.261
	$C_6C_7N_{1a}N_1$	179.694	−179.998	−178.00	−179.960	−179.931	−178.756
	$C_2C_3N_{10}N_{11}$	1.764	−0.229	0.996	4.343	1.883	−1.814
	$C_6C_5C_{12}C_{13}$	−142.923	−161.981	−159.292	−112.810	−135.209	−136.199
	$N_2^-N_1^-C_6^-C_7^-$	−160.657	161.023	−159.227	−166.834	−167.353	−165.640
3	N_3C_4	1.381	1.331	1.381	1.405	1.353	1.413
	C_5C_6	1.462	1.385	1.453	1.455	1.393	1.454
	C_7O_8	1.214	1.338	1.218	1.200	1.354	1.203
	N_9N_{10}	1.279	1.279	1.318	1.263	1.265	1.325
	$N_{10}N_{11}C_3^-C_2^-$	178.850	−179.779	175.332	−29.635	−179.378	−7.945
	$C_6C_7N_{1a}N_1$	179.848	−179.995	−178.321	179.814	179.930	−178.645
	$C_2C_3N_{10}N_{11}$	−0.521	0.038	0.555	0.148	−1.313	1.761
4	N_3C_4	1.382	1.337	1.383	1.403	1.354	1.412
	C_5C_6	1.459	1.385	1.451	1.457	1.393	1.456
	C_7O_8	1.215	1.339	1.219	1.200	1.354	1.203
	N_9N_{10}	1.279	1.280	1.318	1.263	1.265	1.324
	$N_{10}N_{11}C_3^-C_2^-$	178.773	179.633	−175.890	28.007	175.766	8.254
	$C_6C_7N_{1a}N_1$	−179.869	179.963	177.744	−179.627	−179.869	178.746
	$C_2C_3N_{10}N_{11}$	−0.870	−0.106	−0.739	−0.288	1.196	−1.763
	$C_6C_5C_{12}C_{13}$	143.186	163.404	161.144	−116.397	140.751	−143.109

Table 2
Physicochemical features of the different tautomeric forms of compounds **1**–**4**.

Computational level	ΔE			Natural charge at N_{11}			HOMO			LUMO			E_g^a	E_g^b	$\ln_{298}K_I^{oc}$
	NH	OH	hyd	NH	OH	hyd	NH	OH	hyd	NH	OH	hyd			
1															
DFT	0.00	31.39	16.27	−0.260	−0.274	−0.341	−0.196	−0.183	−0.202	−0.072	−0.060	−0.095	2.86	2.47	2.41 (2.07)
DFT (PCM–DMSO)	0.00	27.40	17.56	−0.283	−0.274	−0.316	−0.202	−0.183	−0.206	−0.075	−0.060	−0.096	2.93	2.54	2.37 (1.96)
DFT (PCM – C_2H_5OH)	0.00	28.09	17.81	−0.274	−0.280	−0.316	−0.202	−0.186	−0.206	−0.075	−0.063	−0.096	2.93	2.54	2.40 (1.97)
DFT (PCM – Acetone)	0.00	28.03	17.24	−0.271	−0.286	−0.321	−0.202	−0.189	−0.207	−0.075	−0.065	−0.096	2.93	2.56	2.40 (1.94)
DFT (PCM – $CHCl_3$)	0.00	30.99	16.85	−0.268	−0.281	−0.328	−0.200	−0.186	−0.206	−0.074	−0.063	−0.096	2.91	2.54	2.50 (1.92)
DFT (PCM – CCl_4)	0.00	31.63	17.78	−0.268	−0.281	−0.328	−0.200	−0.186	−0.206	−0.074	−0.063	−0.096	2.91	2.54	2.52 (1.97)
2															
DFT	0.00	26.26	15.75	−0.261	−0.274	−0.339	−0.196	−0.190	−0.202	−0.072	−0.064	−0.097	2.86	2.42	2.37 (2.02)
DFT (PCM–DMSO)	0.00	21.31	13.99	−0.268	−0.293	−0.335	−0.202	−0.193	−0.208	−0.076	−0.072	−0.099	2.91	2.51	2.08 (1.71)
DFT (PCM – C_2H_5OH)	0.00	22.12	14.04	−0.268	−0.293	−0.335	−0.202	−0.193	−0.208	−0.076	−0.072	−0.099	2.91	2.51	2.14 (1.72)
DFT (PCM – Acetone)	0.00	22.42	13.78	−0.271	−0.294	−0.318	−0.202	−0.193	−0.208	−0.076	−0.073	−0.098	2.91	2.54	2.15 (1.70)
DFT (PCM – $CHCl_3$)	0.00	24.73	13.64	−0.265	−0.289	−0.331	−0.198	−0.192	−0.205	−0.074	−0.072	−0.098	2.86	2.47	2.25 (1.69)
DFT (PCM – CCl_4)	0.00	26.41	14.10	−0.265	−0.289	−0.331	−0.198	−0.192	−0.205	−0.074	−0.072	−0.098	2.86	2.47	2.32 (1.72)
3															
DFT	0.00	35.40	31.51	−0.276	−0.293	−0.350	−0.216	−0.204	−0.215	−0.082	−0.069	−0.106	2.86		2.44 (2.61)
DFT (PCM–DMSO)	0.00	28.88	23.63	−0.284	−0.309	−0.344	−0.215	−0.205	−0.218	−0.081	−0.076	−0.102	2.91		2.45 (2.28)
DFT (PCM – C_2H_5OH)	0.00	28.88	26.26	−0.286	−0.303	−0.343	−0.215	−0.205	−0.216	−0.081	−0.076	−0.104	2.91		2.47 (2.30)
DFT (PCM – Acetone)	0.00	31.51	26.26	−0.286	−0.305	−0.333	−0.215	−0.205	−0.217	−0.081	−0.076	−0.102	2.91		2.64 (2.48)
DFT (PCM – $CHCl_3$)	0.00	31.51	26.26	−0.281	−0.302	−0.345	−0.216	−0.204	−0.215	−0.082	−0.074	−0.106	2.86		2.55 (2.34)
DFT (PCM – CCl_4)	0.00	34.13	28.88	−0.278	−0.309	−0.343	−0.216	−0.205	−0.216	−0.082	−0.076	−0.104	2.86		2.61 (2.41)
4															
DFT	0.00	30.96	29.32	−0.276	−0.294	−0.349	−0.215	−0.205	−0.215	−0.082	−0.072	−0.108	3.07		2.40 (2.50)
DFT (PCM–DMSO)	0.00	23.63	21.00	−0.282	−0.310	−0.349	−0.215	−0.206	−0.215	−0.082	−0.079	−0.108	3.07		2.23 (2.12)
DFT (PCM – C_2H_5OH)	0.00	26.26	23.63	−0.283	−0.307	−0.328	−0.215	−0.206	−0.218	−0.082	−0.079	−0.104	3.07		2.28 (2.18)
DFT (PCM – Acetone)	0.00	23.63	21.00	−0.281	−0.299	−0.328	−0.215	−0.202	−0.218	−0.082	−0.075	−0.104	3.07		2.27 (2.15)
DFT (PCM – $CHCl_3$)	0.00	28.88	23.63	−0.280	−0.294	−0.342	−0.215	−0.201	−0.216	−0.083	−0.075	−0.106	3.04		2.37 (2.22)
DFT (PCM – CCl_4)	0.00	28.88	26.26	−0.278	−0.299	−0.342	−0.215	−0.202	−0.216	−0.083	−0.075	−0.106	3.04		2.45 (2.31)

ΔE in kJ/mol, is the energy difference between OH, hydrazone and the NH forms. E_g^a, E_g^b in kcal/mol, are the energy gap between LUMO and HOMO for NH and hydrazone forms, respectively. The equilibrium constant values were obtained from $\ln_{298}\ K^o = -\Delta G^o/RT$ equation.

[c] Values in parentheses represent the $\ln_{298}K_{II}^o$ of the NHNH⇌hydrazone equilibrium. HOMO and LUMO, in ev, indicate the energies of the highest occupied and lowest unoccupied molecular orbitals.

and hydrazone forms are tentatively candidates to exist side by side in appreciable concentrations especially in polar solvents. Even though theoretical calculations in the gaseous phase revealed that OH forms have the highest relative energy values, the difference in these values is still less than 41.84 kJ/mol [64]. A piece of evidence supporting the above finding is the negative values of the calculated HOMO and LUMO energies – following a full geometry optimization – by DFT for all the expected tautomers (Table 2). Illustration of the HOMO and LUMO molecular orbitals for the most stable tautomers (NH) is shown in Fig. 1.

The atomic charge on N_{11} extracted from the natural bond order method (NBO) was calculated to provide an indication of the influence of the substituent at position on one characteristic structural property [51]. Indeed, this method is intently used because it is an efficient method for investigating charge transfer (CT) or hyperconjugative interaction in molecular systems and produces charges that are in agreement with expectations based on the ionization energies of atoms [65]. From Table 2, N_{11} in hydrazone form carries the largest negative charge compared to the other tautomers. On the other hand, it may be noted that increasing the donating character on moving from compound **1** to **2** increases the value of the charge for the OH and hydrazone forms. The situation is completely different in compounds **3** and **4** and this means that the charge on N_{11} is sensitive to the electron-withdrawing character of the terminal heterocyclic moiety.

In fact, the calculation of the equilibrium constants between the above tautomeric structures is very helpful in deciding whether these compounds are more likely to be present in one tautomeric form or a tautomeric mixture.

At first glance the equilibrium constant values depicted in Table 2 suggest that the –OH and –hydrazone forms belonging to compounds **3** and **4** are not likely to exist in the gaseous phase or in solution. The same conclusion can be drawn for the OH tautomers in compounds **1** and **2** as the DFT method yields high values of equilibrium constants for NH–OH tautomerization process. On moving to NH-hydrazone tautomerism in the later compounds (**1** and **2**) especially in polar media, calculations demonstrate an apparent tendency for such equilibrium. This finding is strongly supported by the subsequent results of electronic absorption spectra.

3.2. Electronic absorption spectra in ethanol

The values of λ_{max} and the extinction coefficients (log ε) of the characteristic absorption bands of dyes **1**–**4** in various organic solvents are listed in Table 3. Only the longer wavelength absorption bands are tabulated as the shorter wavelength band remained virtually unaltered in different solvents. Fig. 2 represents the absorption spectra of the studied compounds (**1**–**4**) in ethanol. The bands observed in the range 208–217 nm are due to π–π^* transitions within the terminal heterocyclic fragment. The second band observed in the UV region, in the wavelength range 236–260 nm is attributed to π–π^* transitions within the fused heterocyclic moiety. This assignment is in accordance with the literature data and it is sustained by the slight effect on these transitions by the nature of the terminal heterocyclic moiety [66]. The weak band appearing at around 300 nm in compounds **3** and **4** can be attributed to n-π^* involving the electrons localized on the pyridine nitrogen. Evidence supporting this assignment comes from the disappearance of this band in the acidic medium where excitation of the n-electrons is expected to be hindered by protonation. This adds weight to the suggested chemical structure of the studied compounds. Obviously, the main band in all compounds investigated appears in the range 404–436 nm with a maximum absorption (λ_{max}) depending largely

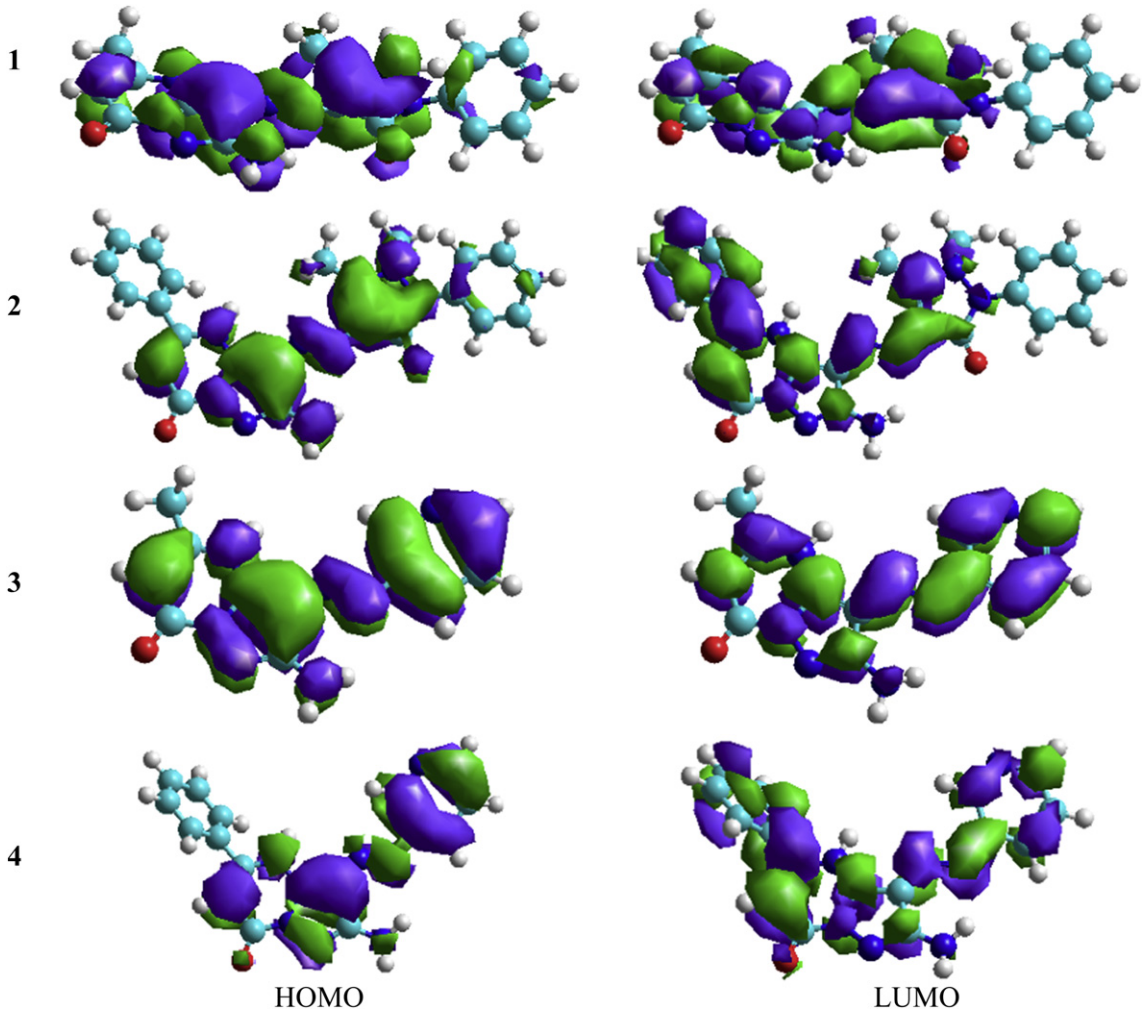

Fig. 1. The highest occupied (HOMO) and lowest unoccupied (LUMO) molecular orbitals of the most stable tautomers (NH).

on their molecular structure. This band can be regarded as a $\pi-\pi^*$ transition involving the π-electronic system throughout the whole molecule with a considerable charge transfer (CT) character. The CT nature of this band is obvious from its broadness [67], the sensitivity of its λ_{max} to the type of the substituent attached and the nature of the solvent (Table 3). This CT originates mainly from the pyrazolo[1,5-*a*]*pyrimidine*-7-(4*H*)-one ring as a donor to the terminal heterocyclic moiety. The characteristic visible electronic

Table 3
Experimental electronic absorption spectral data of compounds **1**–**4**.

Compound	C_2H_5OH		DMF		DMSO		CH_3CN		Acetone		$CHCl_3$		CCl_4	
	λ_{max}	log ε	λ_{max}	log ε	λ_{max}	log ε	λ_{max}	log ε	$\lambda_{max}\lambda$	loλg ε	λ_{max}	log ε	λ_{max}	log ε
1	404	4.48	440	4.38	426	4.29	442	4.34	407	4.33	405	4.38	405_{sh}	4.30
	367	4.56	375_{sh}	4.13	375_{sh}	4.19	367_{sh}	3.88	370	4.38	370	4.46	373	4.38
	246	4.52												
	208	4.61												
2	438_{sh}	4.41	454	4.60	452_{sh}	4.33	438	4.52	448_{sh}	4.02	409	4.49	410	4.47
	415	4.48	372	4.10	423	4.37	372_{sh}	4.08	412	4.46	372	4.55	372	4.55
	374_{sh}	4.36			376_{sh}	4.24			372	4.44				
	257	4.66												
	217	5.10												
3	430	4.26	451	4.25	439	3.99	436	4.19	428_{sh}	3.90	374	4.06	376	4.21
	280	3.80			385	4.02			377	4.02				
	236_{sh}	4.24												
	209	4.58												
4	436	4.48	457	4.54	458	4.41	431	4.45	447	4.46	410	4.27	405	4.24
	297	4.05												
	253	4.57												
	215	4.94												

λ_{max} – position of band maxima in absorption spectra (in nm), ε – absorption coefficients (in $M^{-1}\,cm^{-1}$), sh - shoulder.

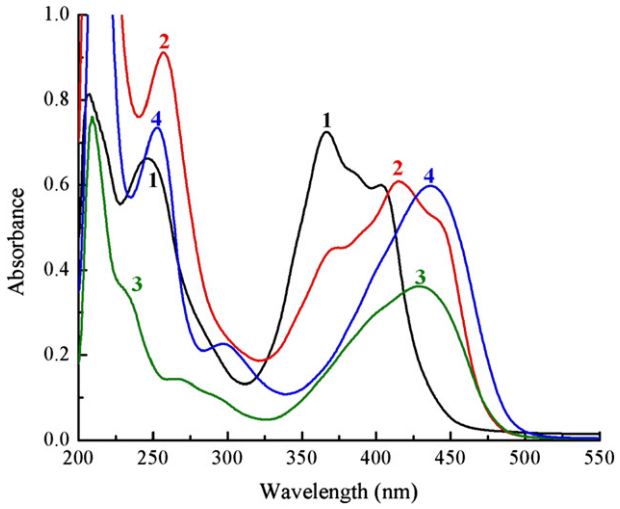

Fig. 2. Electronic absorption spectra of 2.0×10^{-5} M solution of compounds **1**–**4** in ethanol.

bands appearing in the range 367–415 nm in compounds **1** and **2** contain elements characteristic of both NH and hydrazone forms (Fig. 2, Scheme 1). Such tautomerization ability is demonstrated by the composite nature of the main visible band. Therefore, it is possible to assign the shorter wavelength band to $\pi-\pi^*$ transition involving the π-electronic system throughout the whole molecule with a considerable charge transfer (CT) character within the NH tautomer. Meanwhile the longer band can be ascribed to a similar transition within the hydrazone form. On the other hand, the main visible band displayed by compounds **3** and **4** in ethanol and other polar solvents can be attributed to an intramolecular CT within the anionic form (A^-). However, in non-polar solvents, this band can be regarded as a CT transition within the neutral form (NH tautomer). To support the above band assignment, the predicted electronic absorption spectra from time-dependent DFT calculations of the tautomers investigated herein were recorded and the results are gathered in Table 4. On the other hand, the transition energies of the visible absorption (CT) bands of the compounds investigated in ethanol have been determined from λ_{max} values on the basis of the following relation [68] (Table 4):

$$E_T\left(\text{kJ mol}^{-1}\right) = hcN/\lambda = 119.625/\lambda(\text{nm}) \quad (2)$$

On the basis of the predicted electronic absorption spectra, the hydrazone tautomers should show bands at around 415–465 nm in the visible region and the NH forms absorb light strongly at 356–394 nm depending on the molecular structure of the compound investigated. Generally, the above trend – hydrazone forms show bands at high wavelengths relative to NH tautomers – is consistent with the experimental UV–Vis spectra to some extent and the slight deviation may be partly due to solvation effects (Table 4).

Moreover, it is worthy to note that the energy gaps (E_g) between the LUMO and HOMO orbitals for the hydrazone forms are relatively smaller than the corresponding values in the NH tautomers (Table 2). This indicates that the electron transfer from the HOMO orbital to the first excited state (LUMO) is easier in the hydrazone forms. Hence, the NH forms absorb light at relatively low wavelengths in comparison with the hydrazone forms.

Notably, compound **2** exhibits special behavior in polar solvents – a new band at longer wavelength (438 nm) appearing as a clear shoulder. This extra visible band exceeds by far the polarity effect of the solvent and could be attributed to the absorption by the ionized form, though the basic character of ethanol is quite low. This finding occurs on the basis of the well-known acid–base equilibrium ($HA + S \rightleftharpoons A^- + HS^+$) of some other azo dyes, discovered by an examination of their absorption spectra [54–56]. Similar acid–base equilibrium is also recognized in **1** particularly in highly polar solvents and it might be responsible for the disappearance of the prototropic equilibrium in these solvents. Since the tautomeric equilibrium position [A/H] should be influenced by the possibility of interaction with the solvent through charge transfer from solute to solvent as well as the ability of the solvent to form stronger hydrogen bonds with a particular tautomeric form [69]. However, the ionized species predominated in highly polar solvents for compounds **3** and **4**. It is of considerable interest that the appearance of the absorption band due to the ionized form in the polar solvents is because of the high basicity (pK_s) of these solvents compared to non-polar examples [70,71]. Strong evidence verifying such equilibrium in the polar solvents is obtained from two important features namely:

(i) The position of λ_{max} of a solution containing few drops of 1.0 N NaOH is the same as in pure organic solvents; while in a solution containing 1.0 N HCl only the shorter wavelength band appears.
(ii) The color of the dye solution containing NaOH is exactly the same as in pure solvents and widely different from that in solvents containing HCl.

Of particular interest is the positive solvatochromism – reflected in bathochromic shift – in compounds **2** and **4** on going from non-polar to polar solvents (Table 3). This behavior can be explained on the basis that the excited state in these molecules is more polar than the ground state. As a consequence, the energy of the excited state is lowered with increasing the solvent polarity and this produces such a bathochromic shift.

3.3. Spectra in mixed organic solvents

The visible spectra of compounds **1**–**4** in DMF–CCl_4, DMF–$CHCl_3$, DMF–acetone and DMF–C_2H_5OH binary solvent mixtures were undertaken to obtain an insight into the origin of the

Table 4
Wavelengths (λ_{nm}) and oscillator strengths (f) of electronic absorption transitions calculated at TDDFT method and the transition energies of the experimental (CT) absorption bands.

Compound	Time-dependent DFT calculations						E_T (kJ/mol)	
	NH		OH		hyd			
	$\lambda_{(nm)}$	f	$\lambda_{(nm)}$	f	$\lambda_{(nm)}$	f	NH	hyd
1	386	0.62	399	0.78	464	0.52	0.33	0.30
	340	0.18	331	0.12	347	0.08		
	248	0.19	251	0.22	259	0.06		
			214	0.05	217	0.01		
2	394	0.52	429	0.32	415	0.10	0.32	0.29
	343	0.09	378	0.25	361	0.13		
	249	0.19	293	0.16	260	0.26		
	226	0.21	244	0.10	213	0.03		
3	356	0.82	369	0.64	455	0.39	0.28	
	286	0.12	315	0.12	364	0.11		
	212	0.08	262	0.13	342	0.24		
	209	0.11	232	0.40	246	0.09		
4	362	0.74	396	0.45	468	0.28	0.27	
	256	0.04	344	0.55	422	0.18		
	218	0.02	273	0.23	360	0.22		
			218	0.18	256	0.24		
					245	0.10		

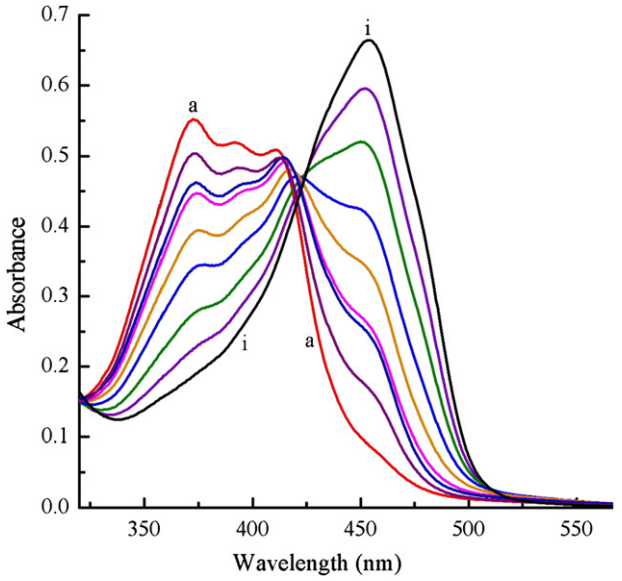

Fig. 3. Visible spectra of 2.0×10^{-5} M solution of compound **2** in DMF–$CHCl_3$ mixture solvents. (a) 1.30 M. DMF (b) 2.59 M. DMF (c) 3.89 M. DMF (d) 5.19 M. DMF (e) 6.49 M. DMF (f) 7.78 M. DMF (g) 9.08 M. DMF (h) 10.38 M. DMF (i) 11.67 M. DMF.

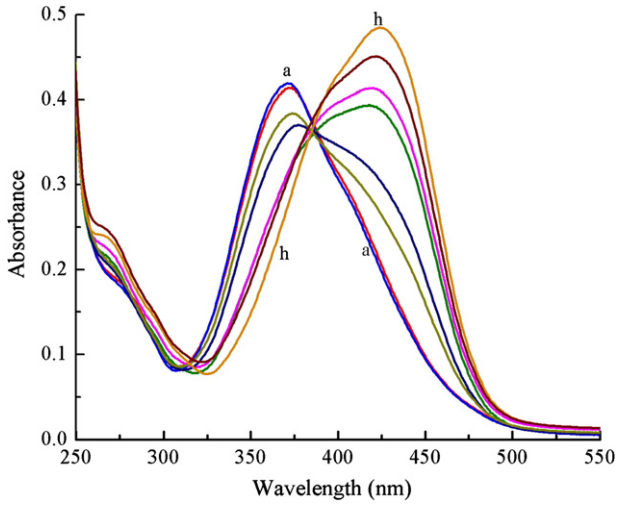

Fig. 4. Electronic absorption spectra of 2.0×10^{-5} M solution of compound **3** in universal buffer solutions containing 20% (v/v) ethanol. pH* (a) 4.56, (b) 4.75, (c) 6.72, (d) 7.00, (e) 7.26, (f) 7.44, (g) 7.51, (h) 8.00.

interaction between these dyes and DMF. This was carried out to find how these compounds, dissolved in highly proton acceptor (DMF), would respond to the presence of successfully increasing amounts of CCl_4, $CHCl_3$, acetone and ethanol. It is evident that in pure DMF the dyes exhibit only one band in the visible region at wavelengths depending upon molecular structure (Fig. 3, Table 3). When the second solvent is added into the solution of the dye in dimethylformamide, the band which previously assigned to the absorption by the ionized form is shifted to a lower wavelength. With the increase of the mole fraction of the added solvent to the binary solvent mixture, the absorption band of the neutral form develops gradually and keeps almost constant at very low levels of DMF. The spectra recorded in all mixed solvents show a fine isosbestic point which indicates the establishment of equilibrium between the ionized and non-ionized forms of the molecule (Fig. 3). This behavior also indicates that DMF molecules have a greater tendency to form ionized forms with solute molecules comparable to acetone and ethanol. The value of the ionization constant (K_{ion}) was determined from the variation of absorbance obtained by decreasing the DMF concentration at a constant wavelength using the following equation [72].

$$\log C_{DMF} = \log K_{ion} + \log(A - A_{min}/A_{max} - A) \quad (3)$$

where A_{min} = absorbance in a low polarity solvent; A_{max} = absorbance in a high polarity solvent (DMF); A = absorbance in the mixed solvent. Gibbs free energy (ΔG) values are obtained by applying eq. (4)

$$-\Delta G = RT \ln K_{ion} \quad (4)$$

The values of ΔG and K_{ion} of the ionization equilibrium existing in solution are cited in Table 5. The negative values of the free energy change of the ionization process indicate that this process is spontaneous. In general, the experimental results presented in Table 5 show that the values of K_{ion} and ΔG of the compounds investigated in mixed solvent are dependent upon R and increase in the following sequence

1 (R=CH_3) > **2** (R=Ph) and **3** ((R=CH_3) > **4** (R=Ph)

3.4. Acid dissociation constants

The acidity constants (pK_a) of the compounds **1**–**4** were determined from their spectral behavior in buffer solutions of varying pH. For this purpose a universal buffer solutions (pH 3.0–12.5) containing 20% (v/v) ethanol to complete ensure solubility of the azo dyes was used. A representative spectrum is shown in Fig. 4. Values of pK_a were determined by making use of three different spectrophotometric methods, namely the half curve-height, the limiting absorbance and the isosbestic point methods [73,74]. The obtained values are reported in Table 6. Generally, it has been found that by increasing the pH value of the medium, the intramolecular CT band exhibits a high red shift in its λ_{max}. This red shift can be explained on the basis that the ionization process facilitates the CT transition-low energy required for such a transition. Beyond any reasonable doubt, the obtained isosbestic point reveals the establishment of equilibrium between the neutral and ionic forms in these compounds. If HA represents the molecule of the azo

Table 5
Values of K_{ion} and $-\Delta G$ for the ionization process of the investigated compounds.

System	Compound							
	1		**2**		**3**		**4**	
	K_{ion}	$-\Delta G$	K_{ion}	$-\Delta G$	K_{ion}	$-\Delta G$	K_{ion}	$-\Delta G$
DMF–C_2H_5OH	11.01	1.42	4.20	0.85	7.52	1.19	5.07	0.96
DMF–acetone	6.84	1.14	5.31	0.96	5.84	1.04	3.41	0.73
DMF–$CHCl_3$	10.78	1.40	6.07	1.10	7.03	1.15	4.65	0.91
DMF–CCl_4	9.79	1.35	3.45	0.73	6.63	1.12	4.21	0.85

Table 6
Values of acidity constants (pK_a) and λ_{max} of the neutral and ionic forms of the compounds **1**–**4**.

Compound	pK_a				SD	λ_{max}, nm	
	Method 1	Method 2	Method 3	Mean		Neutral	Ionic
1	8.67	8.60	8.66	8.64	±0.04	366	425
2	7.38	7.39	7.25	7.34	±0.08	366	430
3	7.23	7.23	7.20	7.22	±0.02	372	425
4	6.32	6.19	6.33	6.28	±0.08	370	429

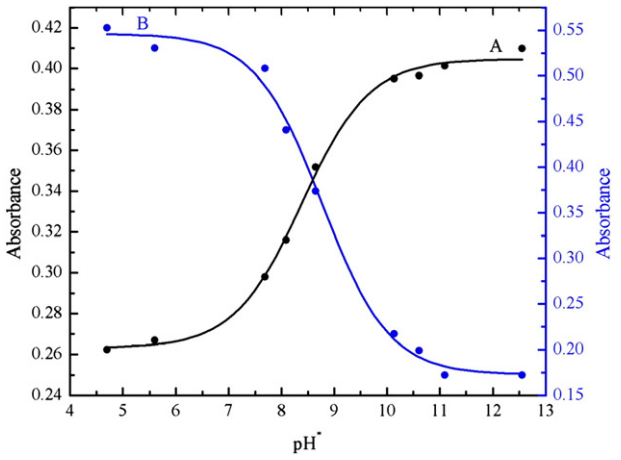

Fig. 5. Absorbance–pH* curve of 2.0×10^{-5} M solution of compound **1** in 20% (v/v) ethanol and water mixture at (A) $\lambda_{max} = 366$ nm and (B) $\lambda_{max} = 425$ nm.

compound, the following equilibrium is found in the universal buffer series.

$$HA \rightleftharpoons A^- + H^+ \quad (5)$$

The constructed absorbance–pH* relations at the selected wavelength are sigmoidal curves shaped, each comprising a clear inflection, indicating typical dissociation processes (Fig. 5). In the light of the determined ionization constant values, the acidity constants (pK_a) increases according to the following sequence:

4 < **3** < **2** < **1**

The decrease in the (pK_a) value is generally in agreement with the increase in the electron releasing ability of the constituent R at C_5 and to withdrawing character of the terminal heterocyclic fragment to the charge transfer.

4. Conclusion

The spectral data generally reveals that compounds **1** and **2** may occur in various accessible tautomeric forms. However, data collected for the two remaining dyes shows only one distinct band in the visible region which may arise from one tautomer. These features of the molecules are reflected in the results obtained from the theoretical calculations, assuming the tautomeric equilibrium between the NH and hydrazone forms co-exists only for **1** and **2**. The other two compounds (**3** and **4**) exist principally in the NH form according to the equilibrium constant values indicated in Table 2. So far, the agreement between the experimental and theoretical results suggests that the DFT/B3LYP/6-31G** method is very powerful in explaining the features and tautomeric phenomena of the compounds under investigation. In the light of the obtained calculations of the energy gap ($\varepsilon_{LUMO} - \varepsilon_{HOMO}$) and time-dependent DFT, the visible absorption bands of compounds **1** and **2** are successfully assigned. The phenyl substituent at C_5 in compound **2** diminishes the energy gap between HOMO and LUMO and consequently absorbs light at relatively long wavelengths compared to compound **1**. The substituents at C_5 have no significant effect on geometrical parameters, but the values of ΔG, K_{ion} of the ionization equilibrium and the acidity constants are significantly affected by the electron donation of the substituents.

Finally, the exponential sensitivity of the studied compounds – their colors change by changing the solvent polarity – strongly suggests their use as analytical reagents to screen different solvents.

Acknowledgment

I would like to express my gratitude to Professor M.H. Elnagdi and Dr. M.A. Selim for providing the samples of the compounds studied. My deepest thanks and appreciations are also due to Professor S.A. Ibrahim and Professor M.F. Aly for their limitless help and fruitful discussions.

References

[1] Gao HW, Liu XH, Qiu Z, Tan L. Non-covalent binding of azo compound to peptide chain: interactions of biebrich scarlet and naphthochrome green with four model proteins. Amino Acids 2009;36:251–60.
[2] Chigrinov V, Prudnikova E, Kozenkov V, Kwok H, Akiyama H, Kawara T, et al. Synthesis and properties of azo dye aligning layers for liquid crystal cells. Liq Cryst 2002;29:1321–7.
[3] Jain VK, Mandalia HC, Bhojak N. Azocalix[4]pyrrole dyes: application in dyeing of fibers and their antimicrobial activity. Fiber Polym 2010;3:363–71.
[4] Cheng YF, Zhao DT, Zhang M, Liu ZQ, Zhou YF, Shu TM, et al. Azo 8-hydroxyquinoline benzoate as selective chromogenic chemosensor for Hg^{+2} and Cu^{+2}. Tetrahedron Lett 2006;47:6413–6.
[5] Pandey A, Singh P, Iyengar L. Bacterial decolorization and degradation of azo dyes. Int Biodeterioration Biodegradation 2007;59:73–84.
[6] Kocaokutgen H, Ozkinali S. Characterisation and applications of some *o,o′*-dihydroxyazo dyes containing a 7-hydroxy group and their chromium complexes on nylon and wool. Dyes Pigments 2004;63:83–8.
[7] Machado AEH, Neto NMB, Ueno LT, de Paula LF, Araujo DMS, Oliveira GS, et al. Study of the spectroscopic properties and first hyperpolarizabilities of disperse azo dyes derived from 2-amino-5-nitrothiazole. J Photochem Photobiol A Chem 2008;199:23–33.
[8] Berg RH, Hvlisted S, Ramanujam PS. Peptide oligomers for holographic data storage. Nature 1996;383:505–8.
[9] Waring DR, Hallas G. The chemistry and application of dyes. New York and London: Plenum Press; 1990.
[10] Buncel E, Rajagopal S. Solvatochromic studies of novel azo dyes. The π_{azo}^* scale of solvent polarity. J Org Chem 1989;54:798–809.
[11] dos Santos AB, Cervantes FJ, van Lier JB. Review paper on current technologies for decolourisation of textile wastewaters: perspectives for anaerobic biotechnology. Bioresour Technol 2007;98:2369–85.
[12] Tezcan H, Tokay N. Synthesis, spectroscopy, and quantum-chemical calculations on 1-substituted phenyl-3,5-diphenylformazans. Spectrochim Acta A 2010;75:54–60.
[13] Huan W. Structural and computational studies of azo dyes in the hydrazone form having the same pyridine-2,6-dione component (II): C.I. Disperse Yellow 119 and C.I. Disperse Yellow 211. Dyes Pigments 2008;79:69–75.
[14] Katritzky AR, Pozharskii AF. Handbook of heterocyclic chemistry. 2nd ed. Oxford: Pergammon/Elsevier Science; 2000.
[15] Elguero J, Katritzky AR, Denisko OV. Prototropic tautomerism of heterocycles: heteroaromatic tautomerism–general overview and methodology. Adv Heterocycl Chem 2000;76:1–84.
[16] Barrow MJ, Christie RM, Monteith JE. The crystal and molecular structures of three diarylide yellow pigments, C.I. Pigments Yellow 13, 14 and 63. Dyes Pigments 2002;55:79–89.
[17] Tauro ST, Countinho E. Azo, hydrazone and other tautomers of azo dye 7-amino-4-hydroxy-3-[(4-methoxy-2-sulfophenyl)azo]-2-naphthalenesulfonic acid: a PM3 study. J Mol Struct 2000;532:23–9.
[18] Sujamol MS, Athira CJ, Sindhu Y, Mohanan K. Synthesis, spectroscopic characterization, electrochemical behaviour and thermal decomposition studies of some transition metal complexes with an azo derivative. Spectrochim Acta A 2010;75:106–12.
[19] Czajkowski W, Stolarski R, Szymczyk M, Wreszcz G. Studies on isomerism of 1:2 iron complexed dye based on 1-($5^{/}$-nitro-$2^{/}$hydroxyphenyl)-3-cyano-5-($4^{//}$-sulphonamidophenyl)formazan. Dyes Pigments 2000;47:143–9.
[20] Wolciechowska M, Wojciechowski G, Wasiak W. Spectroscopic and semi-empirical studies of the phototropic species of 8-amino-5,8-azo-bis-naphthalene-2-sulphonic acid. J Mol Struct 2003;658:125–33.
[21] Ebead YH, Selim MA, Ibrahim SA. Solvatochromic, acid–base features and time effect of some azo dyes derived from 1,3-benzothiazol-2-ylacetonitrile: experimental and semiempirical investigations. Spectrochim Acta A 2010;75:760–8.
[22] Singh A, Chandra M, Sahay AN, Pandey DS, Pandey KK, Mobin SM, et al. Arene ruthenium complexes incorporating immine/azine hybrid-chelating *N–N*\ donor ligands: synthetic, spectral, structural aspects and DFT studies. J Organomet Chem 2004;689:1821–34.
[23] Gopalsamy A, Ciszewski G, Hu Y, Lee F, Feldberg L, Frommer E, et al. Identification of pyrazolo[1,5-a]pyrimidine-3-carboxylates as B-Raf kinase inhibitors. Bioorg Med Chem Lett 2009;19:2735–8.
[24] Elnagdi MH, Elmoghayar MR, Elgemeie GE. Chemistry of pyrazolopyrimidines. Adv Heterocycl Chem 1987;41:319–76.

[25] Anwar FH, Fleita DH, Kolshorn H, Meier H, Elnagdi MH. *2H*-pyrazol-3-ylamines as precursors for the synthesis of polyfunctionally substituted pyrazolo[1,5-a]pyrimidines. Arkivoc 2006;xv:133–41.
[26] Schuurmann G. Modelling pK_a of carboxylic acids and phenols. Quant Struct Act Relat 1996;15:121–32.
[27] Schuurmann G, Cossi M, Barone V, Tomasi J. Prediction of the pK_a of carboxylic acids using the *ab initio* continuum-solvation model PCM-UAHF. J Phys Chem A 1998;102:6706–12.
[28] Frey PA, Kokesh FO, Westheimer FH. A reporter group at the active site of acetoacetate decarboxylase, I. Ionization constant of the nitrophenol. J Am Chem Soc 1971;93:7266–70.
[29] Namazian M, Kalantary-Fotooh F, Noorbala MR, Searles DJ, Coote ML. Møller–Plesset perturbation theory calculations of the pK_a values for a range of carboxylic acids. J Mol Struct 2006;758:275–8.
[30] Ebead YH, Salman HMA, Abdellah MA. Experimental and theoretical investigations of spectral, tautomerism and acid–base properties of Schiff bases derived from some amino acids. Bull Korean Chem Soc 2010;31:850–8.
[31] Ebead YH. The role of the medium on the acid dissociation constants of some azo dyes in view of experimental and theoretical data. J Mol Struct 2010;982:100–6.
[32] Yarlıgan S, Öğretir C, Kaynak B, Esenoğlu E. A study on acid–base properties and hydrogen bonding of some 2-substituted benzimidazole in aqueous phase using semi-empirical methods. J Mol Struct 2002;586:9–16.
[33] Ebead Y, Roshal AD, Wroblewska A, Doroshenko AO, Blazejowski J. Tautomerism of acridin-9-amines substituted at the exocyclic nitrogen atom: spectroscopic investigations and theoretical studies. Spectrochim Acta A 2007;66:1016–23.
[34] Babu DS, Singh WM, Kalita D, Baruah JB. Solvatochromicity of 3-hydroxy-4-(1-(2,4-dihydroxyphenyl)-2-hydroxy-2,2-diphenylethylidene)cyclohexa-2,5-dienone for screening of solvents. Spectrochim Acta A 2010;75:486–9.
[35] Yazdanbakhsh MR, Mohammadi A, Mohajerani E, Nemati H, Nataj NH, Naeemikhah E, et al. Novel azo disperse dyes derived from *N*-benzyl–*N*-ethyl–aniline: synthesis solvatochromic and optical properties. J Mol Liq 2010;151:107–12.
[36] Mahmoud OS. Studies on some pyrazoleamine: the reactivity of some pyrazoleamine compounds under microwave heating. M.Sc. Thesis. Qena, Egypt: South Valley University, Faculty of Science, Department of Chemistry; 2009.
[37] Britton HTS. Hydrogen ions. London: Chapman Hall; 1952. p. 364.
[38] Douheret G. The dissociation of organic compounds in aqueous organic media. I. Determination of the liquid junction potential and the effect of the medium on the hydrogen ion in these systems, and the study of the dissociation of some acid–base couples. Bull Soc Chim Fr 1967;4:1412–9.
[39] Stewart JJP. Optimization of parameters for semiempirical methods V: modification of NDDO approximations and application to 70 elements. J Mol Model 2007;13:1173–213.
[40] Labanowski JK, Andzelm JW, editors. Density functional methods in chemistry. New York: Springer Verlag; 1991.
[41] Baker J. An algorithm for the location of transition states. J Comput Chem 1986;7:385–95.
[42] Schlegel HB, editor. Modern electronic structure theory: geometry optimization on potential energy surfaces. Singapore: World Scientific; 1994.
[43] Hehre WJ, Radom L, Schleyer PVR, Pople JA. Ab initio molecular orbital theory. New York: Wiley; 1986.
[44] Hariharan PC, Pople JA. The influence of polarization functions on molecular orbital hydrogenation energies. Theor Chim Acta 1973;28:213–22.
[45] Becke AD. Density-functional exchange-energy approximation with correct asymptotic behavior. Phys Rev A 1988;38:3098–100.
[46] Becke AD. A new mixing of Hartree–Fock and local density-functional theories. J Chem Phys 1993;98:1372–7.
[47] Lee C, Yang W, Parr RG. Development of the Colle-Salvetti correlation-energy formula into a functional of the electron density. Phys Rev B 1988;37:785–9.
[48] Handy NC, Tozer DJ, Laming GJ, Murray CW, Amos RD. Analytic second derivatives of the potential energy surface. Isr J Chem 1993;33:331–44.
[49] Tomasi J, Persico M. Molecular interactions in solution: an overview of methods based on continuous distributions of the solvent. Chem Rev 1994;94:2027–94.
[50] Barone V, Cossi M, Mennucci B, Tomasi J. A new definition of cavities for the computation of solvation free energies by the polarizable continuum model. J Chem Phys 1997;107:3210–21.
[51] Glendening ED, Reed AE, Carpenter E, Weinhold F. NBO Version 3.1; 2010.
[52] MOPAC 2009, Stewart JJP. Stewart computational chemistry. Version 9.025W web, HTTP://OpenMOPAC.net.
[53] Frisch MJ, Trucks GW, Schlegel HB, Scuseria GE, Robb MA, Cheeseman JR, et al. Gaussian 03, Revision D.01. Wallingford, CT: Gaussian, Inc.; 2004.
[54] Hihara T, Okada Y, Morita Z. Reactivity of phenylazonaphthol sulfonates, their estimation by semiempirical molecular orbital PM5 method, and the relation between their reactivity and azo-hydrazone tautomerism. Dyes Pigments 2003;59:201–22. references therein.
[55] Hammam AM, Rageh NM, Ibrahim SA. Solvatochromic studies on 2-(2-hydroxyphenyl)azol-4-5-diphenylimidazole. Dyes Pigments 1997;35:289–96.
[56] Karcı F, Şener N, Yamaç M, Şener I, Demirçalı A. The synthesis, heterocyclic antimicrobial activity and absorption characteristics of some novel disazo dyes. Dyes Pigments 2009;80:47–52.
[57] Allen FH, Kennard O, Watson DG, Brammer L, Orpen AG, Taylor R. Tables of bond lengths determined by X-ray and neutron diffraction. Part 1. Bond lengths in organic compounds. J Chem Soc Perkin Trans 1987;2:S1–19.
[58] Frizzo CP, Scapin E, Campos PT, Moreira DN, Martins MAP. Molecular structure of pyrazolo[1,5-a]pyrimidines: X-ray diffractometry and theoretical study. J Mol Struct 2009;933:142–7.
[59] Levine IN. Quantum chemistry. 5th ed. Dorling Kindersley (India) Pvt. Ltd., Licensees of Pearson Education in South Asia; 2006. p. 532.
[60] Ji NN, Shi ZQ, Zhao RG, Zheng ZB, Li ZF. Synthesis, crystal structure and quantum chemistry of a novel Schiff base *N*-(2,4-dinitro-phenyl)- $N^{\backslash}$-(1-phenyl-ethylidine)-hydrazine. Bull Korean Chem Soc 2010;31:881–6.
[61] Prikryl J, Lycka A, Bertolasi V, Holcapek M, Machacek V. Structure and reactivity of 3,3-disubstituted 1-(5-nitro-2,1-benzisothiazol-3-yl)triazenes. Eur J Org Chem; 2003:4413–21.
[62] He L, El-Shafei A, Freeman HS, Boyle P. X-ray and molecular modeling studies of 4-[*N*-alkylamino]azobenzene dyes. Dyes Pigments 2009;82:299–306.
[63] Maciejewska D, Wolska I, Kowalska V. The structure of some1-arylazo-2-naphthylamines and their *N*-acetamides deduced from ^{13}C CP/MAS NMR, X-ray crystallography and DFT theoretical calculations. J Mol Struct 2004;693:27–34.
[64] Civcir PÜ. A theoretical study of tautomerism of cytosine, thymine, uracil and their 1-methyl analogues in the gas and aqueous phases using AM1 and PM3. J Mol Struct 2000;532:157–69. references 61, 62 therein.
[65] Glaser R. *Ab* initio quantum-mechanical study of the stability of cyclic α-acetoxy-*N*-nitrosamines: amine *N→NO* dative bonding in α-hydroxy-*N*-nitrosamines versus *N→*carbocation dative bonding in *N*-nitrosiminium ions. J Am Chem Soc 1999;121:5170–5.
[66] Rageh NM. Electronic spectra, solvatochromic behaviour and acidity constants of some 2-amino-3-arylazo-7-hydroxy-5-methyl pyrazolo[1,5-a]pyrimidines. Can J Anal Sci Spectrosc 1997;42:170–7.
[67] Briegleb G. Electron donor–acceptor complex. Berlin: Springer Verlag; 1961.
[68] Laus G, Schottenberger H, Schuler N, Wurst K, Herber RH. A novel solvatochromic 2-nitroacrylonitrile derived from octamethylferrocenecarbaldehyde. J Chem Soc Perkin Trans 2002;2:1445–8.
[69] Wojciechowski K, Szymczak A. The research of the azo–hydrazone equilibrium by means of AM1 method based on the example of an azo dye – the Schaffer salt derivative. Dyes Pigments 2007;75:45–51.
[70] Reichardt C. Solvents and solvent effects in organic chemistry. 2nd ed. Weinheim: VCH; 1990. p. 432.
[71] Coetzee JF, Ritchie CD. Solute solvent interactions. New York: Marcel Dekker; 1969. p. 94.
[72] Issa RM, Ghoneim MM, Idrriss KA, Harfouch AA. Spectrophotometric study of some halogen derivatives of fluorescence in organic solvents of varying polarities. Z Phys Chem (F.M) 1975;94:135–46.
[73] Issa RM, Sadek H, Izzat II. Spectrophotometric studies on dihydric phenols. Z Phys Chem Neue Folge 1971;75:17–25.
[74] Issa RM, Hammam AM, Etaiw SH. Electronic absorption spectra of some 2,3-benzcarbazoloquinones. Z Phys Chem (Leipzig) 1972;78:177–82.